Optics Letters

High purity optical vortex generation in a fiber Bragg grating inscribed by a femtosecond laser

Yali Li,[1,2] Zhiyong Bai,[1,2,*] Zhao Liu,[1,2] Guoxuan Zhu,[1,2] Kaiming Yang,[1,2] Jian Yu,[1,2] Jiayan Chen,[1,2] Cailing Fu,[1,2] Changrui Liao,[1,2] and Yiping Wang[1,2]

[1]Key Laboratory of Optoelectronic Devices and Systems of Ministry of Education/GuangDong Province, College of Physics and Optoelectronic Engineering, Shenzhen University, Shenzhen 518060, China
[2]Shenzhen Key Laboratory of Photonic Devices and Sensing Systems for Internet of Things, Guangdong and Hong Kong Joint Research Centre for Optical Fibre Sensors, Shenzhen University, Shenzhen 518060, China
*Corresponding author: baizhiyong@szu.edu.cn

Received 23 September 2020; revised 11 November 2020; accepted 12 November 2020; posted 13 November 2020 (Doc. ID 410277); published 9 December 2020

In this Letter, a method for orbital angular momentum (OAM) mode generation is proposed and experimentally demonstrated using a fiber Bragg grating (FBG) and off-axis incidence. The FBG fabricated by a femtosecond laser was used to couple the incidence beam into backward high-order modes. The generated modes were then reformed into ring-shaped OAM modes by adjusting the off-axis displacement of the input beam. The intensity distribution, phase vortex, and mode purity of the output light were experimentally investigated. Results indicates that the order of the generated OAM modes is dependent on the resonant wavelength of the FBG, and the sign of the OAM topological charge is determined by the displacement value of the off-axis incident light. In the experiment, ±1- and ±2-order OAM modes were achieved and confirmed, with purities as high as 90%, 91%, 89%, and 88%, respectively.

https://doi.org/10.1364/OL.410277

Orbital angular momentum (OAM) beams carrying helical phase fronts have been extensively studied since their discovery in 1992 [1]. This helical phase is represented as $\exp(il\varphi)$, where l is the topological charge and φ is the azimuthal angle. With the unique character of orthogonality and phase singularity, OAM modes have been widely used in the fields of optical tweezers [2], particle trapping [3], microscopic imaging [4], and quantum information [5]. In recent years, it has also shown great potential in the optical communication field [6,7]. The stable generation of OAM modes is thus a critical task. OAM modes are conventionally generated using cylindrical lens mode converters [8], spiral phase plates [9], q-plates [10], spatial light modulators (SLMs) [11], or silicon integrated devices [12]. However, the inherent advantages of optical fibers, including compactness, low cost, remote delivery, and compatibility with optical communication systems, have produced a growing interest in fiber-based OAM generation.

OAM modes can be directly excited in a fiber using off-axis incident light, which is considered as forming skew rays [13]. This approach is a convenient and simple way to generate OAM and has attracted extensive interest. Inavalli *et al.* [13] achieved various vector vortex modes by changing the launch angle and circular-polarization of the input Gaussian beam, but the conversion efficiency was about 7%, and the largest part of the fundamental mode was left over in the output light. Jin *et al.* [14] off-axis spliced a single-mode fiber (SMF) to a single-ring fiber to excite the vortex modes, and the simulated mode purity was about 80%, but the total coupling efficiency was estimated to be only 7.5%. To improve the conversion efficiency of higher-order modes or the purity of OAM modes, some feasible methods have been proposed. Gao *et al.* [15] reported an off-axis couple between a linearly polarized Gaussian beam and a liquid core fiber. The conversion efficiency was improved to be 37%. Li *et al.* [16] demonstrated an OAM beam generation method by sticking an SMF to a custom-designed two-mode fiber with a certain off-axis and tilt angle. The conversion efficiency of the OAM mode was ∼34%, and the extinction ratio was higher than 20 dB. Although the purity of the OAM mode is improved, fundamental modes generated using off-axis technique must still be filtered out using polarization controllers (PCs) and a polarizer. As such, the low OAM generation purity and conversion efficiency are obvious limitations for the off-axis incidence method, and a simple, high conversion efficiency and high purity OAM mode generation method is still needed.

Grating-based OAM generators possess many advantages in performance, such as high mode conversion efficiency, high mode purity, and flexible wavelength selectivity. There have been various methods [17–19] based on long period fiber gratings (LPFGs) proposed to generate OAMs. However, it is difficult for an LPFG to couple the fundamental mode and higher mode (higher than 1 order). Until recently, the helical LPFG and strong modulation LPFGs [20,21] were achieved to excite ±2- or ±3-order OAMs. Compared with LPFGs, it is easier for the fiber Bragg gratings (FBGs) [22] to excite higher-order modes, which provides a new approach to excite OAM modes with $|l| > 1$. Currently, there is only one method to generate OAM modes based on the FBG, which is the combination of tilted FBGs and PCs [23,24]. OAM generators based on

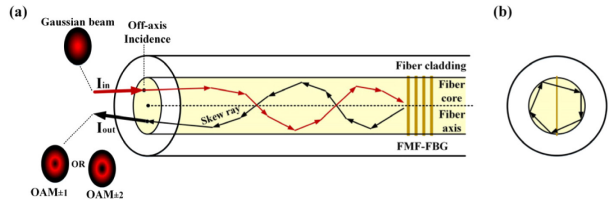

Fig. 1. (a) Schematic diagram of OAM modes generation in the FMF-FBG combined with off-axis incidence. Meridional rays are not shown in the picture. (b) Lateral view of the FMF-FBG.

non-tilted FBGs have not been reported so far. In addition, the previous method based on tilted FBGs and PCs will bring additional effect of polarization on the formed OAM modes, which may bring some inconvenience to the practical application of OAM beams.

In this Letter, an FBG fabricated by a femtosecond laser was combined with off-axis incidence to directly generate OAM modes. The FBG was used to couple the incidence beam into backward high-order modes. The generated modes were reformed into ring-shaped OAM modes by adjusting the off-axis displacement of the input beam. The proposed method not only improves mode purity and conversion efficiency, but also provides a new approach for exciting OAM modes in FBGs, which may avoid the polarized limitation of the OAM modes generation. The working principle for this approach is shown in Fig. 1, where the off-axis incident Gaussian beam (I_{in}) was partly captured by skew rays in a four-mode fiber (FMF). The skew ray propagates along the spiral path in the fiber; that is, its propagation vector possesses a spiral track, and thus, the isophase plane that is perpendicular to direction of the propagation vector is helical, indicating an OAM mode. While propagating through the FMF-FBG, the light was coupled to reverse modes of the same order and higher orders, which inherited the helical phase from the skew rays. A detailed investigation of these helical phase fronts, as well as the topological charge order and purity of excited modes, is presented in this study.

An FMF with a core diameter of 18.5 μm and a cladding diameter of 125 μm was used in the study. Theoretically, this fiber can support LP_{01}, LP_{11}, LP_{21}, and LP_{02} modes for long transmission distances, and could still guide LP_{31} over short lengths. A femtosecond laser (PHAROS, 513 nm/290 fs/200 kHz) was used to inscribe the FMF-FBG via line-by-line scanning, schematically shown in Fig. 2(a). The fiber was fixed on and moved relative to a focused laser beam using a 3D air-bearing motion stage. A 63× oil-immersed objective lens was used to focus the laser on the fiber core, and index matching oil ($n = 1.45$) was selected to eliminate aberrations caused by the fiber's cylindrical shape. A CCD was used to monitor FBG inscription processing in real time. In order to achieve a resonant wavelength near 1550 nm and an increased mode conversion rate, the FMF-FBG fabrication parameters were set as follows. The grating pitch, grating length, scanning line length, and single-pulse energy were 1.070 μm, 1.656 mm, 24 μm, and 19 nJ, respectively. Figure 2(b) shows a microscopic image of an FMF-FBG inscribed using the scanning process discussed above.

An optical spectrum analyzer and a broadband laser source were used to record the FMF-FBG transmission spectrum, as shown in Fig. 3(a). The wavelengths of resonance dips labeled

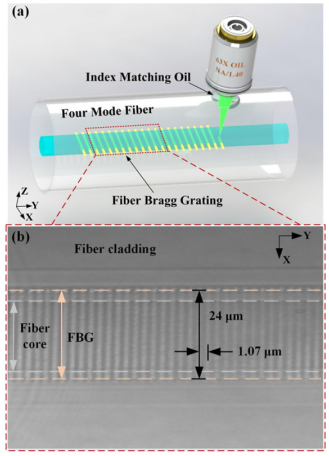

Fig. 2. (a) Schematic diagram of FMF-FBG inscription with a femtosecond laser line-by-line scanning technique. (b) Microscopy images of the inscribed FMF-FBG.

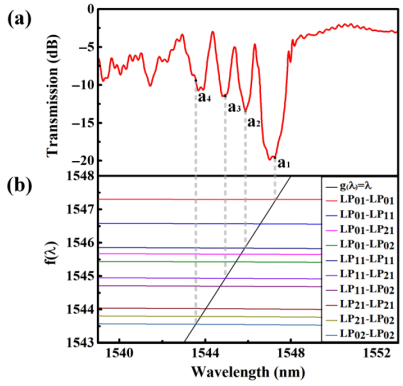

Fig. 3. (a) Transmission spectrum of the FMF-FBG. (b) Theoretical estimates of the resonance wavelengths for corresponding modes, determined by the intersection between $f(\lambda) = (n_{\mathrm{eff},u} + n_{\mathrm{eff},v})\Lambda/2$ and $g(\lambda) = \lambda$. The condition $u = v$ corresponds to self-coupling, while $u \neq v$ indicates cross coupling of different core modes.

a_1, a_2, a_3, and a_4 were 1547.2 nm, 1545.9 nm, 1544.92 nm, and 1543.48 nm, respectively. The insertion loss of the FMF-FBG is −1.97 dB, and the transmission contrasts for the four resonance dips were 17.49 dB, 11.35 dB, 9.34 dB, and 6.72 dB, corresponding to mode conversion efficiencies of 98.2%, 92.7%, 88.4%, and 78.7%, respectively.

In order to clarify the characteristics of the mode coupling in the FMF-FBG, the phase match equation $f(\lambda) = (n_{\mathrm{eff},u} + n_{\mathrm{eff},v})\Lambda/2$ was numerically simulated based on the finite-element method (FEM), where n_{eff} is the effective refractive index for the corresponding mode and Λ is the grating pitch. In this expression $u, v \in \{01, 11, 21, 02\}$, where $u = v$ corresponds to self-coupling and $u \neq v$ indicates cross coupling between two different core modes. We assume $g(\lambda) = \lambda$, and when $g(\lambda) = f(\lambda)$ was met, the resonance in the FMF-FBG occurred. Figure 3(b) demonstrates the curves of $f(\lambda)$ and $g(\lambda)$, and the intersection between them. Comparing the resonant dips of the measured transmission spectra in Fig. 3(a) and intersection positions in Fig. 3(b), the mode coupling patterns

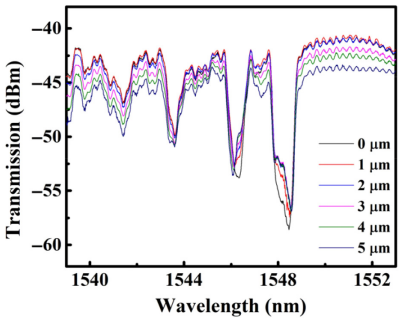

Fig. 4. Transmission spectrum evolution of the FMF-FBG coupled with a launch SMF for varying offsets along the y axis.

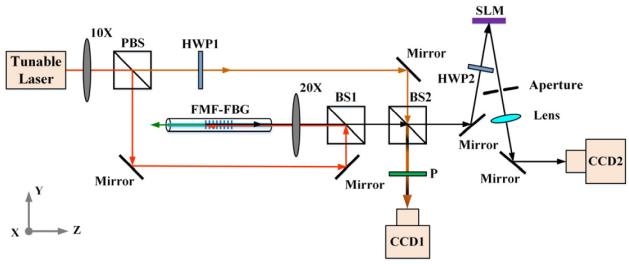

Fig. 5. Experimental setup used for detecting mode intensity distribution of FMF-FBG reflections, characterizing the resulting OAM modes, and measuring the purity of OAM modes. PBS, polarized beam splitter; BS1, beam splitter 1; BS2, beam splitter 2; HWP1, half-wave plate 1; HWP2, half-wave plate 2; P, polarizer; SLM, spatial light modulator.

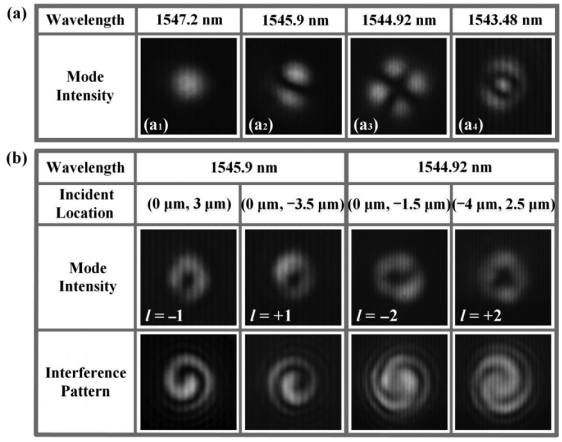

Fig. 6. (a) Intensity patterns for modes at varying resonance wavelengths when coaxis incidence. (b) Intensity patterns and interference patterns for OAM modes generated at different resonance wavelengths and varying incident positions. l represented the topological charge of the helical phase.

can be evaluated. Therefore, from Fig. 3, the wavelengths of resonance dips labeled a_1, a_2, a_3, and a_4 represent mode couplings of $LP_{01} - LP_{01}$, $LP_{11} - LP_{11}$, $LP_{11} - LP_{21}$, and $LP_{02} - LP_{02}$, respectively.

Because the off-axis incidence of light was one of the vital factors in this proposed method, we first investigate the transmission characteristics of the FMF-FBG under lateral offset injection of light. The grating pitch, grating length, scanning line length, and single-pulse energy of FMF-FBG fabrication parameters were 1.070 μm, 1.782 mm, 24 μm, and 16 nJ respectively. The FMF-FBG was aligned with a launch SMF at first, and the transmission spectrum was recorded at a 0 μm offset. A pair of x and y axis motors were then used to produce a series of lateral offsets in the x and y directions. The y axis motor of the launch SMF is moved from 0 to 5 μm in steps of 1 μm, simultaneously recording the transmission spectrum after each step. The transmission spectrum evolution of the FMF-FBG is shown for different y axis offsets in Fig. 4. With the offset value increase, an obvious decrease is observed in intensity, but the resonant wavelength is almost constant. Thus, we can investigate the mode characteristics of the FMF-FBGs with an offset incidence condition near the resonant wavelength from the transmission spectrum in Fig. 3(a).

The experimental setup shown in Fig. 5 was used to study intensity patterns from FMF-FBG reflections, as well as the helical phase. A tunable laser with a wavelength ranging from 1520 to 1630 nm was collimated using a 10× objective lens and divided into two beams by a polarized beam splitter (PBS). The down-path beam reflected from two plane mirrors and a beam splitter (BS1) was focused into the FMF-FBG by a 20× objective Lens. Light reflected by the FMF-FBG then interfered with the reference light of the up-path after passing through a beam splitter (BS2). The resulting intensity distribution and interference patterns were observed by an infrared camera labeled CCD1. A half-wave plate (HWP1) was used to change the polarization direction of the reference beam. A polarizer (P) was used to filter any stray light and keep the two interference beams in the same polarization direction.

The mode intensity patterns at different resonance wavelengths were observed for light at an approximately coaxial incidence into the FMF-FBG, as shown in Fig. 6(a). The modes generated from FMF-FBG reflection are LP_{01}, LP_{11}, LP_{21}, and LP_{02} at the wavelengths of 1547.2 nm, 1545.9 nm, 1544.92 nm, and 1543.48 nm, without generating OAM modes, which agrees well with the stimulation analysis above. At this time, the position of the incidence light was labeled by $(x, y) = (0\ \mu m, 0\ \mu m)$. The z axis position of the incidence light was fixed to ensure the focal plane remained unchanged. The intensity distribution and interference pattern for OAM beams with topological charges of ±1 and ±2 were shown in Fig. 6(b). At the wavelength of 1545.9 nm, the LP_{11} mode is generated by coaxial incident to the FMF-FBG, as shown in Fig. 6(a2). By adjusting the incidence light position to (0 μm, −3.5 μm) and (0 μm, 3 μm), the +1- and -1-order OAM modes are generated at the wavelength of 1545.9 nm. When the incident light position is (0 μm, 0 μm), the LP_{21} mode is generated at the wavelength of 1544.92 nm, as shown in Fig. 6(a3). Similarly, by moving the incidence light position to (−4 μm, 2.5 μm) and (0 μm, −1.5 μm), +2- and -2-order OAM modes are generated at the wavelength of 1544.92 nm, respectively. The results show that OAM can be generated in the reflected light of the FMF-FBG by changing the displacement of off-axis incident light. The off-axis Gaussian beam can be expressed as the superposition of axial Bessel Gaussian (BG) beams [25]. Each BG component represents an azimuthal harmonic with the orbital number m [1]. The FMF-FBG was used to directly couple them into reverse OAM modes.

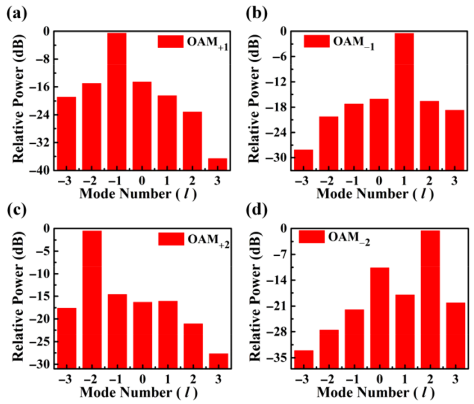

Fig. 7. (a) and (b) Power ratios for each component of the ±1-order OAM modes. (c) and (d) Power ratios for each component of the ±2-order OAM modes, respectively.

After the confirmation of the OAM mode generation, the purities of them were investigated as well. As is shown in Fig. 5, the light reflected by the FMF-FBG, propagating through BS1 and BS2, was incident on a reflective SLM loaded with a series of forked-grating holograms. First-order diffraction spots reflected by the SLM were then recorded by CCD2. The first-order diffracted lights of these holograms has helical phases of $l = -3$, -2, -1, 0, $+1$, $+2$, $+3$, respectively. An OAM beam reflected from the FMF-FBG was converted into a Gaussian beam when a conjugate helical phase was applied. The contribution of each component to the OAM mode was measured by recording the central power of the diffraction spot. The power ratio of each component was then calculated and used to determine the purity of the corresponding OAM mode. A half-wave plate (HWP2) was used to vary the polarization direction of the light, ensuring it was parallel to the polarization response of the SLM. The aperture only passes the first-order diffraction light. The purity results of OAM modes generated at different resonance wavelengths and for varying incident positions are shown in Fig. 7. As seen in Figs. 7(a) and 7(b), the purity of the +1- and -1-order OAM modes was 90.08% and 90.91%, respectively. The purity of the +2- and -2-order OAM modes, shown in Figs. 7(c) and 7(d), was 88.94% and 87.79%, respectively. The purity of the first-order OAM mode is greater than 90%, and the purity of the second-order OAM mode is greater than 88%, which are better than those directly produced by off-axis incident in two-mode fibers [13], single-ring fiber [14], and liquid core optical fiber [15]. The measured purity was lower than the actual one, due to the influence of FMF-FBG end face reflections. An anti-reflective coating could be applied to the fiber end face to improve purity measurement results. Therefore, OAM modes with high purity can be produced by the FMF-FBG and off-axis incidence combination.

A novel technique for directly generating OAM modes using an FBG, assisted by off-axis incidence, has been proposed and experimentally demonstrated. By controlling off-axis displacement value and selecting incident light wavelengths, ±1- and ±2- order OAM modes were generated and confirmed in an FMF. The purity of the ±1- and ±2-order OAM modes produced in this experiment was as high as 90%, 91%, 89%, and 88%, respectively. The proposed methodology is simple, controllable, and offers a high conversion efficiency and high purity, which can be used to excite higher-order OAM modes and can also be applied to a laser or OAM-based system.

Funding. National Natural Science Foundation of China (61635007, 61875134, 61905155, 62005169); Guangdong Natural Science Foundation (2017A030310033, 2018KQNCX219); Shenzhen Science and Technology Innovation Commission (JCYJ20170412105604705, JCYJ20180507182058432); Research Funding from Shenzhen University (2019097).

Disclosures. The authors declare no conflicts of interest.

REFERENCES

1. L. Allen, M. W. Beijersbergen, R. J. Spreeuw, and J. P. Woerdman, Phys. Rev. A **45**, 8185 (1992).
2. M. Padgett and R. Bowman, Nat. Photonics **5**, 343 (2011).
3. M. Cen, M. Mazilu, Y. Arita, E. M. Wright, and K. Dholakia, Opt. Lett. **38**, 4919 (2013).
4. L. Ya, P. Gregg, E. Karimi, A. Rubano, L. Marrucci, R. Boyd, and S. Ramachandran, Optica **2**, 900 (2015).
5. A. Mair, A. Vaziri, G. Weihs, and A. Zeilinger, Nature **412**, 313 (2001).
6. H. Hung, G. Xie, Y. Yan, N. Ahmed, Y. Ren, Y. Yue, D. Rogawski, M. J. Willner, B. I. Erkmen, K. M. Birnbaum, S. J. Dolinar, M. P. J. Lavery, M. J. Padgett, M. Tur, and A. E. Willner, Opt. Lett. **39**, 197 (2014).
7. J. Wang, Photon. Res. **4**, B14 (2016).
8. J. Courtial and M. J. Padgett, Opt. Commun. **159**, 13 (1999).
9. M. W. Beijersbergen, R. P. C. Coerwinkel, M. Kristensen, and J. P. Woerdman, Opt. Commun. **112**, 321 (1994).
10. G. Biener, A. Niv, V. Kleiner, and E. Hasman, Opt. Lett. **27**, 1875 (2002).
11. G. C. Berkhout, M. P. Lavery, J. Courtial, M. W. Beijersbergen, and M. J. Padgett, Phys. Rev. Lett. **105**, 153601 (2010).
12. X. L. Cai, J. Wang, M. J. Strain, B. Johnson-Morris, J. Zhu, M. Sorel, J. L. O'Brien, M. G. Thompson, and S. Yu, Science **338**, 363 (2012).
13. V. V. G. Krishna Inavalli and N. K. Viswanathan, Opt. Commun. **283**, 861 (2010).
14. X. Jin, F. Pang, Y. Zhang, S. Huang, Y. Li, J. Wen, Z. Chen, M. Wang, and T. Wang, IEEE Photon. Technol. Lett. **28**, 1581 (2016).
15. W. Gao, X. Hu, C. Mu, and P. Sun, Opt. Express **22**, 11325 (2014).
16. S. Li, Z. Xu, R. Zhao, L. Shen, C. Du, and J. Wang, IEEE Photon. J. **10**, 6601607 (2018).
17. Y. Zhao, Y. Liu, L. Zhang, C. Zhang, J. Wen, and T. Wang, Opt. Express **24**, 6186 (2016).
18. W. Zhang, K. Wei, L. Huang, D. Mao, B. Jiang, F. Gao, G. Zhang, T. Mei, and J. Zhao, Opt. Express **24**, 19278 (2016).
19. S. Li, Q. Mo, X. Hu, C. Du, and J. Wang, Opt. Lett. **40**, 4376 (2015).
20. H. Zhao, P. Wang, T. Yamakawa, and H. Li, Opt. Lett. **44**, 5370 (2019).
21. X. He, J. Tu, X. Wu, S. Gao, L. Shen, C. Hao, Y. Feng, W. Liu, and Z. Li, Opt. Lett. **45**, 3621 (2020).
22. M. M. Ali, Y. Jung, K. S. Lim, M. R. Islam, S. U. Alam, D. J. Richardson, and H. Ahmad, IEEE Photon. Technol. Lett. **27**, 1713 (2015).
23. Y. Zhao, C. Wang, Z. Liu, K. Zhou, C. Mou, Y. Liu, L. Zhang, and T. Wang, in *Asia Communications and Photonics Conference (ACP)* (2017), paper S3A, p. 3.
24. K. Yang, Y. Liu, Z. Wang, Y. Li, Y. Han, H. Zhang, and B. Mao, Opt. Fiber. Technol. **55**, 1068 (2020).
25. M. Vasnetsov, V. Pas'Ko, and M. Soskin, New J. Phys. **7**, 46 (2005).